Kir4.1 channel activation in NG2 glia contributes to remyelination in ischemic stroke

Xiaoqi Hong,[a,b,e] Yujin Jian,[a,b,e] Shenghao Ding,[c,e] Jianpo Zhou,[c] Xiaoli Zheng,[a,b] Huimin Zhang,[a,b] Butian Zhou,[a,b] Canbin Zhuang,[c] Jieqing Wan,[c,**] and Xiaoping Tong[a,b,d,*]

[a]Songjiang Institute and Songjiang Hospital, Shanghai Jiao Tong University School of Medicine, Shanghai, China
[b]Department of Anatomy and Physiology, Shanghai Jiao Tong University School of Medicine, Shanghai, China
[c]Department of Neurosurgery, Renji Hospital, Shanghai Jiao Tong University School of Medicine, Shanghai, China
[d]Shanghai Research Center for Brain Science and Brain-Inspired Intelligence, Shanghai, China

eBioMedicine
2023;87: 104406
Published Online XXX
https://doi.org/10.1016/j.ebiom.2022.104406

Summary

Background Stroke is one of the most common neurological diseases in the world and is clinically manifested by transient or permanent brain dysfunction. It has a high mortality and disability rate, which severely affects people's health and diminishes the quality of life. However, there is no efficient treatment that can be considered curative and there are other less well-known theories of pathogenesis. Therefore, it is imperative to gain a full understanding of the pathophysiology of ischemia and to seek new therapeutic strategies.

Methods We first examined Kir4.1 channel and myelin based protein (MBP) expression in brain tissues from acute ischemic patients by Western blotting. We then established a transient ischemic mouse model (tMCAO) to conduct molecular, cell biological, transmission electron microscopy and pharmacokinetic studies, as well as in Kir4.1 cKO mice. Finally, neuroimaging and behavioral analyses were used to examine whether activation of Kir4.1 channel by luteolin could contribute to neuronal functional recovery in ischemic stroke.

Findings In acute ischemic stroke patients, we first demonstrated that Kir4.1 ion channels were greatly impaired and a severe demyelination of axons occurred in ischemic infarction area of cerebral cortex in these patients. Further evidence showed that the deficits of Kir4.1 channels in NG2 glia led to the myelin loss of axons in a transient ischemic mouse model (tMCAO). Treating ischemic mice with a natural botanical extract, luteolin augmented Kir4.1 channel currents in NG2 glia and consequently promoted remyelination of axons, alleviated the infarction area and ultimately improved motor function in a series of behavioral tests.

Interpretation Targeting Kir4.1 ion channels expressed in NG2 glial cells by luteolin treatment highlights an effective therapeutic strategy for a prompt brain functional recovery in ischemic stroke.

Funding This work was supported by grants from the Ministry of Science and Technology China Brain Initiative (2022ZD0204702, to X.T.), the National Natural Science Foundation of China (82271466, 82171279, 31970904 and 31571063), the Program for Professor of Special Appointment (Eastern Scholar for Dr. X.T.) at Shanghai Institutions for Higher Learning (1510000084), Shanghai Pujiang Talent Award (15PJ1404600), Shanghai Municipal Science and Technology Major Project (2018SHZDZX05) and Shanghai Science and Technology Project (17411954000).

Keywords: Kir4.1 ion channels; NG2 glia; Ischemic stroke; Luteolin; Remyelination; Neuronal functional repair

*Corresponding author.
**Corresponding author.
E-mail addresses: xtong@shsmu.edu.cn (X. Tong), jieqingwan@126.com (J. Wan).
[e]These authors contributed equally.

Research in context

Evidence before this study

Ischemic stroke, accounting for 87% of all strokes, is clinically manifested by transient or permanent brain dysfunction and causes axonal demyelination and ultimately neuronal cell death. There is no efficient treatment that can be considered curative or disease-modifying. Recent studies demonstrated that glial cells play a crucial role in the pathogenesis of ischemia. In particular, the deficits of Kir4.1 channels expressed in NG2 glia potently induced myelin loss in a transient ischemic mouse model (tMCAO) of stroke. However, whether this pathological finding occurs in ischemic patients and seeking a potential therapeutic target of Kir4.1 channels remains undiscovered.

Added value of this study

In the present study, we report that Kir4.1 channels and MBP expression are severely reduced in the infarction area of the cerebral cortex of acute ischemic patients, as well as in ischemic stroke model mice. Further evidence demonstrates that the deficits of Kir4.1 channels in NG2 glia but not in astrocytes lead to myelin loss of axons in a transient ischemic mouse model (tMCAO), which can be faithfully replicated in Kir4.1 conditional knockout mice. Treating ischemic mice with a natural flavonoid, luteolin augments Kir4.1 channel currents in NG2 glia and consequently promotes remyelination of axons, reduces the infarction area, improves sensorimotor functional recovery, and prolongs the lifespan of ischemic injured mice.

Implications of all the available evidence

There is currently lack of effective targets or strategies for drug design as treatment options for most ischemic stroke patients. Our findings provide new evidence that Kir4.1 ion channel impairment exacerbates ischemic pathology and their activation ameliorates demyelination of axons and thus highlights a promising drug candidate, luteolin as a Kir4.1 channel activator for the treatment of ischemic stroke.

Introduction

Stroke is a neurological disease clinically manifested by transient or permanent brain dysfunction. As one of the three most common diseases in the world, stroke has a high mortality and disability rate, which severely affects people's health and diminishes quality of life. Ischemic stroke is the most common form, accounting for 87% of strokes. Ischemic stroke mainly causes impairment of neural cells and ultimately the loss of brain function due to ischemia and hypoxia. Although intravenous thrombolysis has been reported to be beneficial for a small population of younger patients within 4.5 h after acute ischemic stroke onset, the treatment options for most stroke patients to date are very limited and there are no treatments that can be considered curative.[1–3] Therefore, it is imperative to gain a full understanding of the pathophysiology of ischemia and to seek new therapeutic strategies.

In the central nervous system (CNS), neurons have very limited self-renewal or regeneration capability when they are damaged or injured in adulthood. Therefore, it is currently important to realize that the concept of brain protection in the treatment of ischemic stroke patients has been changed from reducing neuronal cell death to activating endogenous neuroprotection. With this goal in mind, we recently discovered that the inwardly rectifying K^+ channel subtype Kir4.1 ion channels expressed in NG2 glia, one type of glial cell population which is crucial to sustain the differentiation of myelinating oligodendrocytes and actively interact with neuronal synapses in the brain, are necessary for myelin formation during early brain development in mice.[4–6] However, it remains unclear whether Kir4.1 channels are impaired in ischemic human patients and what is the impact on neuronal functional recovery by simply targeting Kir4.1 channels expressed in NG2 glia.

Kir4.1 has been well studied in astroglia and oligodendrocyte lineage cells in the CNS. These channels play prominent roles in the maintenance of resting membrane potential (RMP), extracellular K^+ uptake, sensing the local K^+ levels, cell volume regulation, facilitation of glutamate uptake, as well as in brain disorders such as Huntington's disease, white matter injury and ischemia.[5,7–13] Although there is no pharmacologically specific blocker of Kir4.1 channels, low dosage barium (100 μM) has been found to efficiently block 80% of Kir4.1-induced currents in rodents.[5,9,11] However, a pharmacological activator of Kir4.1 channels has not been reported to date. Since the reduction of Kir4.1 channel-induced currents mostly occurs in numerous brain diseases that have been investigated, it becomes more urgent and necessary to seek an alternative Kir4.1 channel activator for a potential therapeutic treatment.

We therefore started to investigate whether Kir4.1 channels and myelin-related protein expression are altered in the cortex of individuals with acute ischemic stroke who were diagnosed by CT (Computed Tomography) brain scans and post-surgery pathological examination. We found that, consistent with our previous and present findings in a transient ischemic mouse model (tMCAO), Kir4.1 ion channel protein expression was dramatically reduced and a severe myelin loss occurred

in ischemic patients as well. We also discovered that luteolin, a natural botanical extract, can specifically augment Kir4.1 channel currents in NG2 glia and thus ameliorate the infarction area, promote remyelination of axons and improve the motor function in ischemic stroke model mice. Thus, targeting Kir4.1 ion channels in NG2 glial cells sheds light on a new pathway for neuronal protection and luteolin administration provides a therapeutic avenue for the clinical treatment of ischemic stroke.

Methods

Animals

All animal procedures complied with the animal care standards set forth by the US National Institutes of Health (Protocol number: A-2018-028) and were approved by the Animal Ethics Committee of Shanghai Jiao Tong University School of Medicine (AAALAC accreditation Unit, 001670). All mice were kept on a C57BL/6 background and under a 12 h–12 h light–dark cycle with food and water provided *ad libitum* from the cage lid.

Pdgfrα-creER™ (RRID: IMSR_JAX:000664), Kir4.1$^{f/f}$ (RRID: IMSR_JAX: 026826) and Rosa26-mGFP (RRID: IMSR_JAX: 007676) were obtained from the Jackson Laboratory (U.S.A.). C57BL/6 J mice (RRID: IMSR_JAX:000664) were obtained from the Slac Laboratory Animal (Shanghai, China). To induce Cre recombinase in Pdgfrα-creER™; Kir4.1$^{f/f}$ mice, 120 mg/kg tamoxifen (ABCONE, T56488-5G) dissolved in corn oil (ABCONE, AOB100669) was intraperitoneally injected for 5 consecutive days starting from the postnatal day 10. To induce Cre recombinase in Pdgfrα-creER™; Rosa26-mGFP mice, 120 mg/kg tamoxifen was intraperitoneally injected for 5 consecutive days between postnatal day 45 and 60.

Human tissue samples

Human tissue was obtained directly from the surgery room and rapidly frozen in oxygenated ice-cold high sucrose slice dissection buffer containing (in mM): 26 NaCl, 2.5 KCl, 1.3 $MgCl_2$, 8 $MgSO_4$, 1.25 NaH_2PO_4, 26 $NaHCO_3$, 10 D-glucose and 208 sucrose and then stored at –80 °C for Western blotting. Human tissue collection and use were approved by the human ethical committee in Renji Hospital, Shanghai Jiao Tong University School of Medicine, China (Reference No. 2017-078). Written informed consent for sample collection was obtained from all the study participants. For infarct surgical specimens, we freshly removed infarct tissue from patients diagnosed with acute ischemia. For control (non-ischemic) specimens, we freshly removed normal/healthy tissues from surgical patients diagnosed with intracranial hemorrhage, intractable epilepsy, glioblastoma or metastatic brain tumors. In brief, from epileptic surgical patients, we collected the normal/healthy tissue adjacent to the removed seizure focus while the patients underwent respective surgery; from neuro-oncology patients, we collected the paracancerous tissue as normal/healthy tissue.[14] Patient information was provided in Tables S1 and S2. The average age of the ischemic group was 55.7 ± 6.9 years (n = 6) and for the control group, it was 45.6 ± 6.7 years (n = 10), p = 0.3433, two-tailed unpaired t-test.

tMCAO model in mice

The experimental protocols were approved by the Animal Care and Use Committee of Shanghai Jiao Tong University School of Medicine.[5] The brain transient focal ischemia was induced by suture occlusion of the middle cerebral artery (MCAO) in seven- to eight-week-old male mice, including wild-type (WT) (~25 g), Pdgfrα-creER™; Rosa26-mGFP (~25 g) and Pdgfrα-creER™; Kir4.1$^{f/f}$ mice (~15 g) with congenic C57BL/6 background. Rectal and temporalis muscle temperature was maintained at 37 ± 0.5 °C with a thermostatically controlled heating pad and lamp. Mice were anesthetized and a suture of 0.105 mm in diameter with a 0.2-mm-diameter tip (Jia-Ling Biological Technology, China) was inserted into the internal carotid artery (ICA) through a cut of the external carotid artery to occlude the MCA for 40 min. Regional cerebral blood flow was monitored by laser Doppler flowmetry (VMS-LDF2; Moor Instruments Ltd, UK). Mice showing less than 20% reduction in cerebral blood flow at the core regions of the MCA territory were excluded from the study.

Acute brain slice preparation

For the preparation of brain slices, P40-60 mice were deeply anesthetized and intracardially perfused with oxygenated ice-cold dissection buffer containing (in mM): 82.75 NaCl, 2.4 KCl, 6.8 $MgCl_2$, 0.5 $CaCl_2$, 1.4 NaH_2PO_4, 23.8 $NaHCO_3$, 23.7 D-glucose and 65 sucrose. Coronal hippocampal slices were cut at 300 μM thickness (VT1200S; Leica Microsystems, Germany) and allowed to equilibrate for at least 1 h at 31 °C in aCSF containing (in mM): 125 NaCl, 2.5 KCl, 1 $MgCl_2$, 2 $CaCl_2$, 1.25 NaH_2PO_4, 25 $NaHCO_3$, and 12.5 D-glucose. All the buffers in this experiment were continuously bubbled with a mixture of 95% O_2/5% CO_2 gas.

Construction of pLVX-Kcnj10-IRES-mCherry plasmid

The plasmid pLVX-Kcnj10-IRES-mCherry was obtained by subcloning the human Kcnj10 cDNA (NM_002241.5) into the vector pLVX-IRES-mCherry (Takara, No. 631237) using the XbaI and BamHI restriction sites and was verified by sequencing before the transfection. The primers for Kcnj10 amplification were listed as follows: Forward (XbaI): 5′GCTCTAGAATGACGTCAGTTGC CAAGGTG3′, Reverse (BamHI): 5′CGGGATCCTC

AGACATTGCTGATGCGCAC3′ (Sangon Biotech, Shanghai, China).

For the transfection, the pLVX-Kcnj10-IRES-mCherry plasmid was diluted at the calculated concentration by OPTIM-MEM (Gibco, MA, USA) and transfected into the HEK293T cells (RRID: CVCL_0063) with lipofection 2000 reagent (Thermo Fisher Scientific Inc., Waltham, MA, USA) according to manufacturer's instructions.

Cell culture

HEK-293T cells were purchased from ATCC and were not further authenticated. Cells were maintained in Dulbecco's modified Eagle's medium (DMEM) supplemented with 10% fetal bovine serum (FBS) and 1% penicillin/streptomycin (P/S) at 37 °C in humidified 5% CO_2 incubator. One day before whole-cell patch clamp recordings, cells were digested in 0.25% trypsin. HEK-293T cells were transfected Kcnj10 plasmids by Lipofectamine 2000 (Invitrogen) following the manufacturer's instructions. On the day of electrophysiological recordings, HEK-293T cells expressing Kir4.1 channels were dissociated and triturated. Cells were not cultured beyond 20 passages.

For primary NG2 glial cells culture,[6] E14 mouse cortices tissues were diced into ~1 mm^3 pieces in a 60 mm dish with a sterilized razor blade. The minced tissues were transferred to digestion solution [trypsin solution, 0.25% (Gibco, Baltimore, MD); Dnase I, 75 U/ml (Worthington, Lakewood, NJ)] and incubated for 10 min in the tissue culture incubator at 37 °C. The cells were collected by centrifugation in a swinging bucket at 1000 *g* for 5 min. The pellet was resuspended with freshly prepared neurosphere growth medium (Dulbecco's Modified Eagle Medium (DMEM)/F12 supplemented with B27 (Gibco, Baltimore, MD) and 10 ng/ml EGF (Peprotech, Rocky Hill, NJ)) and added 5×10^5/ml cells to the dishes. Half of the medium was replaced with a fresh neurosphere growth medium for 8–10 days every 2 days. After the neurospheres formed, the EGF containing neurosphere growth medium was changed to oligosphere medium (DMEM/F12 supplemented with B27, 10 ng/ml platelet-derived growth factor (PDGF, Peprotech, Rocky Hill, NJ), 10 ng/ml bFGF (Novus Bio, Centennial, CO). After the oligospheres formed for 7–9 days, the spheres were continuously digested by trypLE (Gibco, Baltimore, MD) and OPCs/NG2 cells were plated at 5×10^5/ml on a new PDL-coated dish in OPC medium (DMEM/F12 supplemented with B27, N2 (Gibco, Baltimore, MD)), 0.1% BSA, 10 ng/ml PDGF, 20 ng/ml bFGF, 5 μg/ml IGF (R&D Systems, Minneapolis, MN).

For primary astrocytes culture, mouse cortices from 2-day-old postnatal mice were dissociated by trypsin solution and plated as a single-cell suspension in DMEM medium supplemented with 10% fetal bovine serum. After 6–7 days, or once the primary cultures are confluent, microglia were removed by shaking the cells at 240 rpm for 3 h, and then the cells were shaken at 240 rpm for overnight in order to remove oligodendrocytes. After that, the purified astrocytes were dissociated and seeded for the subsequent experiments.

Electrophysiological recordings from acute brain slices and cultured cells

For brain slice whole-cell patch clamp recordings, an individual slice was placed in the recording chamber and continuously perfused with oxygenated aCSF at room temperature. Slices were visualized with an upright epifluorescent microscope (BX51WI, Olympus, Tokyo, Japan) equipped with differential interference contrast optics and an infrared CCD camera (optiMOS, Q IMAGING, Olympus, Tokyo, Japan). All the electrophysiological recordings were made in hippocampal CA1 region with a MultiClamp 700B amplifier (Molecular Devices, Sunnyvale, CA, USA). Signals were low-pass filtered at 2 kHz and sampled at 20 kHz using Digidata 1550A (Molecular Devices) and data were collected 2 min after obtaining a stable whole-cell configuration. Patch pipettes were pulled from borosilicate glass capillaries with a microelectrode puller (Model P-1000, Sutter Instruments).

For NG2 glia patch recordings, hippocampal slices (300 μM thick) were prepared from 45 to 60 day-old transgenic mice conditionally expressing green fluorescent protein (GFP) on NG2 glia under the control of Pdgfrα promoter (Pdgfrα-creER™; Rosa26-mGFP mice). Glass pipettes with a resistance of 6–8 MΩ were filled with a low chloride intracellular solution containing (in mM): 125 K-gluconate, 15 KCl, 8 NaCl, 10 HEPES, 0.2 EGTA, 3 Na_2-ATP, and 0.3 Na-GTP (pH to 7.3). Cells were held at –80 mV in voltage clamp mode.

For whole-cell recordings of hippocampal CA1 astrocytes, hippocampal slices (300 μM thick) were prepared from 45 to 60 day-old C57/BL6 mice. Glass pipettes with a resistance of 6–8 MΩ were filled with a low chloride intracellular solution (see NG2 glia patch recordings). Cells were held at –80 mV in voltage clamp mode.

For whole-cell recordings of cultured cells, HEK-293T cells were transfected with pLVX-Kcnj10-IRES-mCherry or control vector for 24 h. Only pLVX-Kcnj10-IRES-mCherry or pLVX-IRES-mCherry positive HEK-293T cells were used for whole-cell patch recordings. Glass pipettes with a resistance of 2–3 MΩ were filled with a high chloride intracellular solution containing (in mM): 130 KCl, 2 $MgCl_2$, 0.5 $CaCl_2$, 2.5 Na_2-ATP, 0.3 Na-GTP, 10 HEPES and 1 EGTA (pH to 7.3 with KOH). Cells were held at –70 mV in voltage clamp mode. The external solution contained (in mM): 150 NaCl, 10 Glucose, 10 HEPES, 2 $CaCl_2$, 5 KCl, 1 $MgCl_2$, pH adjusted to 7.3 with

Tris-base. 100 μM $BaCl_2$ was added into the bath to block Kir4.1 channel currents in all experiments.

Pharmacokinetics and permeability analysis

As described previously, mice were i.p. injected with 35 mg/kg luteolin (Cat. No. L107329; aladdin).[15,16] Blood samples (0.1 mL) were collected from the suborbital vein into heparin tubes at 0, 0.25, 0.5, 1, 2, 4, 8, 12 h after treatment. The blood was immediately centrifuged at 4000 *g* for 10 min to separate out plasma.

To determine whether peripheral administration of luteolin could penetrate the blood brain barrier and enter the brain, the brain tissues of mice that were administered with 35 mg/kg of luteolin for 9 days were collected and frozen at –80 °C. Brain homogenates were prepared and analyzed for total luteolin by HPLC[17] at the Core Facility of Basic Medical Sciences, Shanghai Jiao Tong University School of Medicine.

Viral vector injections

To selectively knock out Kir4.1 in astrocytes, 4 week-old Kir4.1$^{f/f}$ mice were injected with a Cre-dependent AAV vector: AAV2/5-gfaABC1D-EGFP-P2A-iCre-WPRE-pA (Cat. No.S0407-5; Taitool Bioscience). Mice were anesthetized with isoflurane, and placed in an animal stereotaxic apparatus (STOELTING, USA). The viral vector was stereotaxically injected in the motor cortex. The injection coordinates relative to bregma were as follows: anteroposterior, 0.9 mm; mediolateral, 1.45 mm; dorsoventral, –1.45 mm below the surface. A total of 400 nL (1E+13 V.G./mL) AAV vector were injected into the M1 region.[18] Subsequent experiments were performed 3 weeks after the virus injection.

Transmission electron microscopy

Tissue processing and image acquisition by transmission electron microscopy (EM) were carried out as previously reported.[19] In brief, all mice were anesthetized and perfused through the ascending aorta with cold 0.1 M PBS for ~3 min and then followed by ice-cold mixture of 4% PFA and 0.1% glutaraldehyde in 0.1 M PB (pH 7.4) for ~5 min. Brains were dissected and post-fixed overnight by immersion in the same fixative at 4 °C. After that, the sections were rinsed in phosphate buffer and immersed in a solution of 1% osmium tetroxide in phosphate buffer for 1 h, then rinsed in phosphate buffer and gradually dehydrated on a series of ethanol from 30% to 70%. Then, the sections were stained with a solution of 1% uranyl acetate in 70% ethanol for 1 h and further dehydrated in ethanol. After dehydration was completed, the sections were cleared in propylene oxide and infiltrated with Epon resin (EMBED 812; Electron Microscopy Sciences) overnight at room temperature. The following day the sections were flat-embedded in new Epon resin and allowed to polymerize in an oven at 60 °C for 72 h. Ultrathin sections (90 nm thick) were obtained using a Leica EM UC6 ultramicrotome (Leica Microsystems, Wetzlar, Germany). The slices were observed and photographed by TEM (Tecnai Spirit Bio-Twin) with an accelerating voltage of 120 kV at the Center of Cyro-Electron microscopy, Zhejiang University.

Protein extraction and Western blots

All mice were anesthetized and brains rapidly removed and placed into ice-cold PBS. Fresh tissue including the hippocampus was rapidly dissected bilaterally in ice-cold PBS under ×10 magnification (Zeiss) and tissue samples were rapidly frozen on dry ice. Total protein was extracted from individual tissue samples using a lysis buffer containing: 50 mM Tris HCl, 150 mM NaCl, 1% NP-40, 0.5% deoxycholate, 0.1% SDS, protease inhibitors cocktail (Cat. No. 04693132001; Roche), pH 7.6, tissue was ground until it was completely broken into a homogenate and centrifuged at 12,000 rpm for 20 min at 4 °C. The lysates were centrifuged to remove the insoluble deposit and the supernatants were measured with a BCA kit (Thermo Fisher Scientific, USA). The supernatants were denatured at 65 °C for 30 min. For human brain tissue, brain protein samples obtained from Renji Hospital were swiftly placed into the lysis buffer and the same operation described above was repeated. The entire process was performed on dry ice.

The extracted proteins were separated on a Tris-glycine gel and transferred into polyvinylidene difluoride membranes (BIO-RAD #162-0177), which were blocked for 2 h in TBS-T (TBS with 0.1% Tween 20, pH 7.6) containing 3% bovine serum albumin (BSA) (BBI Life Sciences, A600332-0100) and incubated with primary antibody at 4 °C overnight. The primary antibodies used for Western blotting were rabbit anti-Kir4.1 (Alomone Labs Cat# APC-035, RRID: AB_2040120), mouse anti-MBP (Millipore Cat# MAB382, RRID: AB_94971), and mouse anti-β-actin (Thermo Fisher Scientific Cat# MA5-15739, RRID: AB_10979409). The membranes were subsequently washed with TBS-T and incubated for 2 h with HRP-conjugated anti-rabbit or anti-mouse immunoglobulin G (1:5000) at room temperature. Western blots were visualized using Clarity™ Western ECL Substrate (Bio-Rad, Hercules, USA) and exposed to the Tanon Chemiluminescence imaging system. Equivalence of protein loading was corrected by probing for β-actin. For quantification, the optical density of the gel bands was determined using ImageJ Software v1.30 (US National Institutes of Health).

Immunohistochemistry and image analysis

For immunohistochemistry, mice were anesthetized and perfused through the ascending aorta with a solution of normal saline for ~3 min, followed by 4% paraformaldehyde in 0.1 M PB for 5 min. Brains were

removed and post-fixed in 4% paraformaldehyde at 4 °C overnight and then cut into 30-μM-thick coronal sections including cortex and hippocampus. These free-floating sections were incubated in permeable buffer (0.3% Triton X-100 in PBS) for 15 min and then blocked with donkey serum (Ruite Biotechnology, w9030-05) (5% in PBS-T: PBS with 0.1% TritonX-100) for 2 h at room temperature. After that, sections were incubated with primary antibodies, described below, overnight at 4 °C. Sections were washed with PBS + 0.1% Triton X-100 three times for 15 min each and then placed in blocking solution containing secondary antibodies for 2 h at room temperature. Sections were incubated with DAPI (1:1000, Cell Signaling 4083S) for 15 min.

The primary antibodies included Chicken antibody to GFP (Abcam Cat# ab13970, RRID:AB_300798), Rabbit anti-PDGFRα (R&D Systems, Cat# AF1062, RRID: AB_2236897), Chicken anti-GFAP (Abcam, Cat# ab4674, RRID: AB_304558), Rat antibody to CD68 (Bio-Rad Cat# MCA1957, RRID:AB_322219), and Rabbit antibody to Iba-1 (Abcam Cat# ab178847, RRID:AB_2832244). The corresponding secondary antibodies included Donkey anti-Rabbit Alexa Fluor 488 (Thermo Fisher Scientific Cat# A21206, RRID:AB_2535792), Goat anti-Chicken IgG 488 (Thermo Fisher Scientific Cat# A-11039, RRID:AB_2534096), Goat anti-Rat IgG 647 (Thermo Fisher Scientific Cat# A11039, RRID:AB_141778). Sections were incubated with 4′,6′-diamidino-2-phenylindole dihydrochloride (DAPI, 1:1000, Cell Signaling 4083S) for 15 min to label nuclei at room temperature and mounted on glass slides in Fluoromount Aqueous Mounting Medium (AQUA-MOUNT, REF 13800). All slice images were acquired on a Leica TCS SP8 confocal microscope with HC PL APO CS2 ×10/air objective. The images of different channels were thresholded and image analysis was performed by Image-Pro Plus (Media Cybernetics).

Superoxide dismutase (SOD) activity assays

Mice were sacrificed by decapitation and the brains were immediately dissected. Brain tissues were rapidly homogenized, and clarified lysates were obtained by centrifugation (12,000 *g* for 5 min) at 4 °C. Supernatants were isolated and reacted with SOD assay kit (Beyotime, S0101, China) at 37 °C for 25 min according to manufacturers' protocols. The SOD activity was normalized to protein level.

TUNEL assay

In order to assess apoptosis levels in the M1 and CA1 areas, TUNEL histochemistry was performed according to the instructions provided by commercial kit manufacturer (*in situ* Cell Death Detection, TMR red, Roche; Germany). Animals were anesthetized and perfused through the ascending aorta with a solution of normal saline for ~3 min, followed by 4% paraformaldehyde in 0.1 M PB for 5 min. Brains were removed and post-fixed in 4% paraformaldehyde at 4 °C overnight and then cut into 30-μM-thick coronal sections including cortex and hippocampus. These frozen sections were incubated in permeable buffer (0.3% Triton X-100 in PBS) for 15 min at room temperature. Then the sections were incubated with TUNEL reaction mixture for 60 min at 37 °C in a chamber with moderate humidity, rinsed with PBS. Sections were incubated with DAPI (1:1000, Cell Signaling 4083S) for 15 min. TUNEL positive cells were acquired on a Leica TCS SP8 confocal microscope equipped with HC PL APO CS2 ×20/0.75 DRY objective at the Core Facility of Basic Medical Sciences, Shanghai Jiao Tong University School of Medicine. Image analysis was performed by ImageJ 1.52a (US National Institutes of Health). The images of different channels were thresholded, cell numbers were determined according to the DAPI channel threshold image.

Luteolin delivery and behavioral assessment following stroke

Luteolin (HPLC > 98%) was purchased from Shanghai Aladdin Biochemical Technology. It was dissolved in dimethylsulfoxide (DMSO) to make stock solution and was kept at −20 °C. The stock solution was diluted with proper saline solution. The final concentration of DMSO in the bath was <0.1%.[20]

Mice (n = 6–9 per group) were evaluated on the grid-walking test, rotarod test and corner test as described. Baseline behavior was established 3 days prior to the stroke and the mice were administered with 35 mg/kg of luteolin or 0.9% saline intraperitoneally, once daily, for 9 days. Behavior was assessed at 1, 3, 6- and 9-days following stroke.

Grid-walking test

The grid-walking task was used to evaluate mice sensorimotor function impairment after stroke.[21] Mice were placed in a grid area (35 cm/25 cm/40 cm) (length/width/height) with a mesh size of 15 mm and allowed to walk freely for 5 min. A foot fault was recorded if the left limb dropped into the grid hole or if the mouse rested on the grid at wrist level. The total number of footsteps and foot faults were recorded by investigators blinded to the mouse groups. The percentage of foot faults was calculated using the following formula: foot faults/(foot fault + non-foot fault steps) × 100%.

Corner test

The corner test was used to evaluate neurological function in terms of sensorimotor and postural asymmetries.[22] Mice were placed facing an entry at the corner between two boards joined at a 30° angle. When the mouse reached the wedge of the corner, it would then rear and turn either to the right or the left. Twenty trials

were performed for each mouse. The number of right or left turns was recorded. The percent of ipsilateral turns was calculated.

Rotarod test

To assess motor function after stroke,[23] mice were tested on a Rotarod (AccuRotor Rota Rod, Accuscan Instruments, Inc.) accelerating from 4 to 40 rpm in 300 s. The maximum duration of every trial was 5 min, and a minimum 5 min break was given between trials. After 2 days of training, the mice were tested on the Rotarod on Day 3. Mice were subjected to 5 trials/day for 3 consecutive days. Only mice that stayed on the accelerating rotarod (4–40 rpm for 300 s) were considered as experimental subjects. At 1, 3, 6- and 9-days following stroke, mice were tested 3 times at an accelerating speed from 4 to 40 rpm for 300 s and the mean duration was calculated. Results were expressed as the time (seconds) spent on the rotarod and reflected the motor function.

mNSS score

The procedure was conducted as described before with slight modifications.[24] At 1, 3, 6- and 9-days following stroke, mNSS was used to assess neuro-deficits, which comprise a set of terms to evaluate various aspects of neurological function, including motor function (muscle and abnormal movement), sensory function (visual, tactile, and proprioceptive), and reflexes (pinna, corneal, and startle reflexes). The range of mNSS score was from 0 to 16. One point was given when a mouse failed to perform a test or lacked a tested reflex.

Neuroimaging

Infarct volumes were assessed in live mice using a 7T small-animal MRI (BioSpec70/20USR) at 1, 3, 6-and 9-days following stroke in this study. Mice were anesthetized by inhalation through a face mask of 1.0–2.0% isoflurane in 70% N_2O and 30% O_2. During the scanning procedure, a small-animal monitoring and gating system (SA Instruments) kept measuring the animal's respiration *via* a pillow sensor placed under the abdomen. T2-weighted images were acquired to detect infarct volume, with scan parameters applied as follows: TR = 3000 ms; effective TE = 60 ms; and RARE factor = 8. A total of 20 slices were acquired with thickness = 0.5 mm; field of view = 2.56 cm × 2.56 cm; matrix, 128 × 128; and the total scanning time for a single brain is about 3 minutes and 12 seconds. MRI data were analyzed using the 3D slicer software.

Ethics

All animal procedures complied with the animal care standards set forth by the US National Institutes of Health (Protocol number: A-2018-028) and were approved by the Animal Ethics Committee of Shanghai Jiao Tong University School of Medicine (AAALAC accreditation Unit, 001670). Human tissue collection and use was approved by the human ethical committee in Renji Hospital, Shanghai Jiao Tong University School of Medicine, China (Reference No. 2017-078). Written informed consent for sample collection was obtained from all the study participants.

Statistical analysis

All statistical tests were run in GraphPad InStat 3. The graphs were created in Origin 8 and assembled in CorelDraw 12. Data are presented as mean ± s.e.m. For each set of data to be compared, we determined in GraphPad InStat whether the data were normally distributed or not. If they were normally distributed, we used parametric tests, as listed in the text. If the data were not normally distributed, we used non-parametric tests, as indicated in the text. Paired and unpaired Student's two tailed t-tests (as appropriate and as indicated in the text), parametric ANOVA with Tukey–Kramer multiple comparisons test and non-parametric ANOVA with Kruskal–Wallis test were used for most statistical analyses. For electrophysiological experiments, n values represent the number of recorded cells. For all biochemistry, n values represent the number of mice. For immunohistochemistry, n values represent the number of brain slices. For behavioral experiments, n values represent the number of tested mice. Investigators were blinded to the groups or samples during the experiments. No statistical methods were used to pre-determine sample size, or to randomize. Statistical significance was set at $*p < 0.05$, $**p < 0.01$, $***p < 0.001$.

Role of the funding source

The funding sources had absolutely no involvement in the study design, collection, analysis and interpretation of data, manuscript preparation and the decision to submit the paper for publication.

Results

Kir4.1 and MBP deficits in both ischemic human patients and tMCAO mice

We obtained infarct cortical tissues from 6 patients who underwent surgery for acute ischemic stroke and normal/healthy tissue samples from an additional group of 10 patients who underwent surgery for intracranial hemorrhage, intractable epilepsy or neuro-oncology as a comparison (Tables S1 and S2). In brief, from epileptic surgical patients, we collected the normal/healthy tissue adjacent to the removed seizure focus while the patients underwent resective surgery; from neuro-oncology patients, we collected the paracancerous tissue as normal/healthy tissue. Every patient had a well-defined clinical

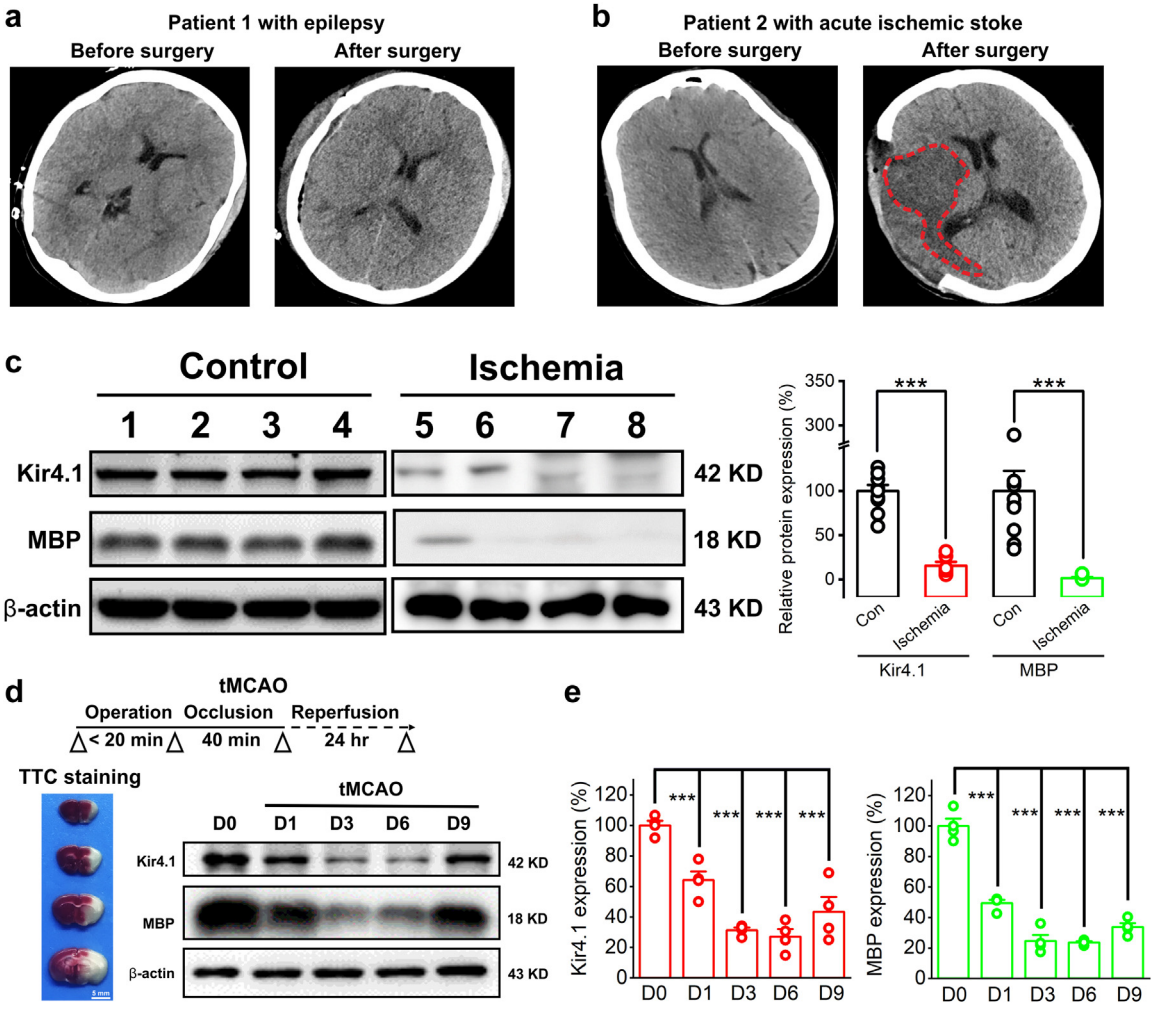

Fig. 1: Deficits of Kir4.1 and MBP expression in both ischemic human patients and tMCAO mice. (a and b) Representative CT brain scans show an epileptic patient before and after the resective surgery (a) and an acute ischemic patient before and after decompressive craniectomy (b). The high density contrast area marked with red dotted line confirms the cerebral infarction of the ischemic stroke patient after decompressive craniectomy. (c) Representative images (left panel) and summary bar graph (right panel) of Kir4.1 and MBP expression levels from 10 non-ischemic surgical patients as comparison and 6 acute ischemic stroke patients, respectively. There is a significant decrease of Kir4.1 and MBP expression in ischemic cerebral tissues compared with that in non-ischemic patients. n = 6 and 10 patients for each group, respectively. ***p < 0.001, two-tailed unpaired t-test. (d) The experimental diagram illustrates an established transient middle cerebral artery occlusion (tMCAO) mouse model of ischemic stroke. After MCA occlusion for 40 min, 2,3,5-triphenyltetrazolium chloride (TTC) staining was observed after 24 h reperfusion to detect the extent of the infarction in a series of brain sections. Representative images of Kir4.1 and MBP expression levels of ipsilateral infarction region by Western blottings at day 0, 1, 3, 6, and 9 of the onset of tMCAO. (e) The summary bar graphs show the expression changes of Kir4.1 and MBP in a 9-days time window of tMCAO. Note that both Kir4.1 and MBP show a continuous decrease starting at 24 h after reperfusion of tMCAO, while after the sixth day, they both rebounded synchronously. ***p < 0.001. n = 4 mice for each group, one-way analysis of variance (ANOVA) followed by Bonferroni *post-hoc* tests.

diagnosis by CT scans and pathological examinations (two examples are shown in Fig. 1a and b). In light of previous findings in ischemic rodents,[5] we first examined the expression of inwardly rectifying potassium channels subtype Kir4.1 protein and myelin based protein (MBP) in ischemic patient brain tissues by Western blotting analysis. Compared with non-ischemic brain tissues obtained from control patients, we found a dramatic reduction of MBP in infarct region of ischemic brains, which indicated a severe demyelination occurred in these patients (100 ± 22.7% for control vs. 1.54 ± 1.1% for ischemia, n = 10 for control group, n = 6 for ischemia group, p < 0.001, two-tailed unpaired t-test, Fig. 1c). Moreover, a significant decrease of Kir4.1 channel proteins was observed in ischemic brain tissues (100 ± 11.89% for control vs. 16.03 ± 5.42% for

ischemia, n = 10 and 6 for control group and ischemia group, respectively, p = 0.0052, two-tailed unpaired t-test, Fig. 1c). To further confirm this, we introduced an established transient middle cerebral artery occlusion (tMCAO) mouse model of ischemia (Fig. 1d). After 24 h ischemia reperfusion, both Kir4.1 and MBP expression showed a significant decrease in ipsilateral infarct area compared with its contralateral side in tMCAO mice (Kir4.1 expression: 100 ± 4.38% for sham control vs. 64.32 ± 8.05% for tMCAO at day 1, p < 0.001, Tukey–Kramer multiple comparisons test; MBP expression: 100 ± 6.85% for sham control vs. 51.6 ± 0.28% for tMCAO at day 1, p < 0.001, Tukey–Kramer multiple comparisons test, n = 4 mice per group, Fig. 1d and e). We also observed an obvious reduction of these two proteins in a 9-day progression period after the onset of tMCAO (Fig. 1d and e). Taken together, the results showed significant deficits of Kir4.1 and MBP in human patients and tMCAO model mice when exposed to the hypoxic or ischemic injury.

Impairment of Kir4.1 ion channels in NG2 glia leads to myelin loss of axons in tMCAO mice

We next investigated the correlation between the Kir4.1 impairment and the myelin loss observed in human ischemic stroke and tMCAO model mice. As Kir4.1 ion channels mostly express in astroglia and oligodendrocyte lineage cells including NG2 glia,[5,8,11,12,25] we started to compare the functional change of Kir4.1 channels in both NG2 glia and astrocytes of tMCAO mice. In agreement with the decrease of Kir4.1 protein in infarct and penumbral region of tMCAO mice, the Ba^{2+}-sensitive Kir4.1 channel currents were largely reduced by 97.86% in ipsilateral NG2 glia compared with a 1.66% reduction in ipsilateral astrocytes after ischemia in Pdgfrα-CreER™;mGFP mice (Kir4.1 currents in NG2 glia: contralateral, −542.06 ± 49.08 pA, n = 7 cells, vs. ipsilateral, −11.59 ± 6.04 pA, n = 6 cells at a holding voltage of −150 mV, p < 0.001, two-tailed unpaired t-test, Fig. 2a–c; Kir4.1 currents in astrocytes: contralateral, −755.22 ± 115.83 pA, n = 8 cells, vs. ipsilateral, −742.70 ± 90.97 pA, n = 8 cells at a holding voltage of −150 mV, p = 0.9334, two-tailed unpaired t-test, Fig. S1), which suggested that functional impairment of Kir4.1 channels mainly occurred in NG2 glia but not in astrocytes after ischemia.[5,6] In addition, both macroscopic K^+ channel currents and Ba^{2+}-sensitive Kir4.1 currents in ipsilateral NG2 glia showed a continuous loss at day 9 following ischemic stroke (contralateral, −542.06 ± 49.08 pA, n = 6 cells, vs. ipsilateral, −11.59 ± 6.04 pA, n = 6 cells at a holding voltage of −150 mV, p < 0.01, two-tailed unpaired t-test, Fig. S2).

With the aid of electron microscopy, we further assessed the direct impact of Kir4.1 channels on myelination in tMCAO mice as well as in Kir4.1 cKO mice. As shown in Fig. 2d–f and i, the thickness of myelin sheaths and G-ratio of myelinated axons were clearly impaired in ipsilateral cortex compared with its contralateral side in tMCAO mice (myelin sheath thickness after tMCAO: contralateral, 221.43 ± 7.22 nm, vs. ipsilateral, 143.49 ± 4.85 nm, p < 0.001, Tukey–Kramer multiple comparisons test; G-ratio of myelinated axons after tMCAO: contralateral, 0.7137 ± 0.0096, vs. ipsilateral, 0.8416 ± 0.005, p < 0.001, Tukey–Kramer multiple comparisons test, n = 78 axons in contralateral and 94 axons in ipsilateral cortex from 4 wild type mice). This impairment of myelin sheath thickness was replicated by solely knocking down of kcnj10-encoded Kir4.1 expression in NG2 glia (myelin sheath thickness: 132.61 ± 14.67 nm in ipsilateral tMCAO in wild type mice vs. 138.79 ± 7.13 nm in contralateral tMCAO in Pdgfrα-CreER™;$Kir4.1^{f/f}$ mice, p > 0.05, Tukey–Kramer multiple comparisons test, n = 94 axons in ipsilateral WT cortex and n = 44 axons in contralateral Kir4.1 cKO cortex, respectively, Fig. 2d, e, g and h). Moreover, the demyelination was aggravated in ipsilateral cortex of Pdgfrα-creER™;$Kir4.1^{f/f}$ mice compared with that of wild type mice after ischemia (Fig. 2d, g and i). However, conditional knockdown of Kir4.1 in astrocytes by injection of Cre-dependent AAV vector (AAV2/5-gfaABC1D-EGFP-P2A-iCre) into $Kir4.1^{f/f}$ mice cortex did not show any alterations in myelin sheath thickness and G-ratio of myelinated axons compared with its contralateral side (myelin sheath thickness: contralateral, 221.91 ± 4.29 nm, vs. ipsilateral, 222.48 ± 4.40 nm, p = 0.9116, Mann–Whitney unpaired test; G-ratio of myelinated axons: contralateral, 0.7125 ± 0.007, vs. ipsilateral, 0.7241 ± 0.006, p = 0.5080, Mann–Whitney unpaired test, n = 84 axons in contralateral and 92 axons in ipsilateral cerebral cortex, Fig. 3a–d). In summary, the results demonstrated that Kir4.1 channels expressed in NG2 glia are essential for the myelination and contribute to myelin loss in ischemic stroke.

Luteolin increases Kir4.1 ion channel currents and promotes remyelination in tMCAO mice

Luteolin (3,4,5,7-tetrahydroxy flavone, Lut) is one of the most prevalent flavones, which is naturally present in many vegetables, fruits and medicinal plants.[26,27] It has been recently reported that luteolin augments both Kv and Kir currents in coronary arterial smooth muscle cells to prevent coronary arterial spasm,[20] which prompted us to investigate whether luteolin can be a potential target of Kir4.1 channel opening in NG2 glial cells as there is no pharmacological Kir4.1 channel activator available to date. We first transfected Kir4.1 plasmids in HEK-293T cells and found significant increases of both Kir4.1 channel protein by Western blot and Kir4.1-induced currents in a voltage–current relationship by electrophysiology (Fig. S3a–e). After application of different doses of luteolin at 10, 50, 100 and

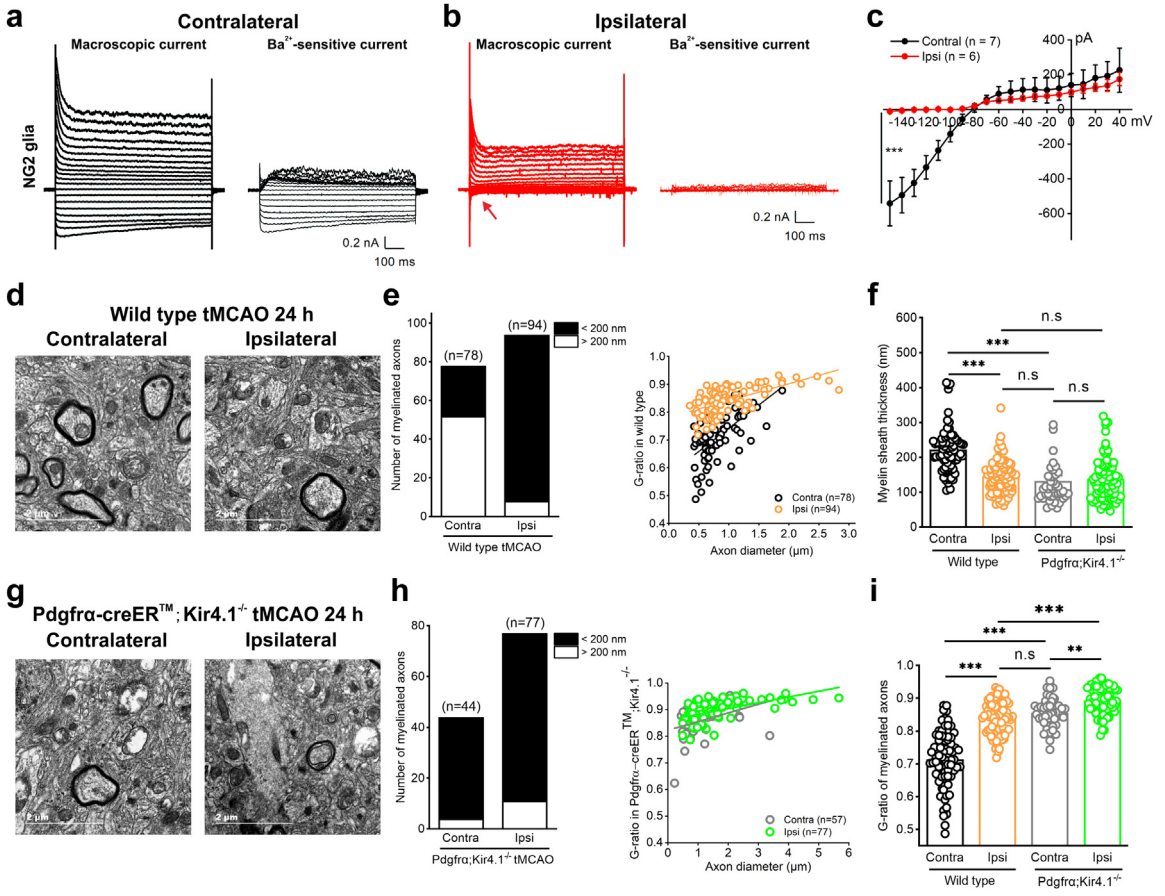

Fig. 2: The impairment of Kir4.1 channels expressed in NG2 glia leads to myelin loss in axons from tMCAO mice. (a and b) Representative traces show macroscopic currents and Ba^{2+}-sensitive currents in NG2 glia in both contralateral (a) and ipsilateral (b) hippocampal CA1 regions of tMCAO. The arrow shows a dramatic loss of Ba^{2+}-sensitive Kir4.1 current in ipsilateral NG2 glia after tMCAO. (c) Average I/V plot is for Ba^{2+}-sensitive currents in NG2 glia after tMCAO. The error bars represent s.e.m. ***p < 0.001, two-tailed unpaired t-test. n indicates the number of cells recorded. (d) Electron micrographs demonstrate the presence of impaired axons with demyelination in ipsilateral cortex compared with its contralateral region after 40 min tMCAO in wild type mice at postnatal 8 weeks. In contralateral cortex of tMCAO, axons show normal myelin, which exhibits dark, ring-shaped sheaths surrounding the axon. Scale bars: 2 μM. (e) Bar graph and G-ratio of myelinated axons represent the number of myelinated axons and G-ratio between ipsilateral cortex after tMCAO with its contralateral side. n indicates the number of axons from 4 wild type mice. (f) The box-plots represent average of myelin sheath thickness in both wild type mice and Kir4.1 deficient mice after tMCAO. The data were normally distributed and statistical significance was assessed within each group using Tukey–Kramer multiple comparisons test. ***p < 0.001, n.s indicates not significant. The analyzed axons are from 4 mice per group. (g and h) Electron micrographs (g), bar graph and G-ratio of axonal diameter (h) show the demyelinated axons in both contralateral and ipsilateral hippocampus after 40 min tMCAO in Pdgfrα-CreER™;$Kir4.1^{f/f}$ mice at postnatal 8 weeks. Scale bars: 2 μM. (i) The box-plots represent the average of G-ratio of myelinated axons in both wild type mice and Kir4.1 deficient mice after tMCAO. The data were normally distributed and statistical significance was assessed within each group using Tukey–Kramer multiple comparisons test. **p < 0.01, ***p < 0.001, n.s indicates not significant. The analyzed axons are from 4 mice per group.

150 μM, we found that 100 μM luteolin induced a maximum net increase of Kir4.1 currents in transfected HEK-293T cells (Fig. S3f and g). Therefore, we chose 100 μM luteolin for the following examinations in acute brain slices. To further illustrate how luteolin directly affects Kir4.1 channels in glial cells *in situ*, we analyzed the net increase of Ba^{2+}-sensitive Kir4.1 currents in both hippocampal NG2 glia and astrocytes. In astrocytes, the net increases of Ba^{2+}-sensitive Kir4.1 currents were: 25.63 ± 1.29% for basal vs. 35.31 ± 4.44% for 100 μM luteolin when the cell voltage was held at −150 mV (p = 0.0619, two-tailed unpaired t-test, n = 9 and 10 cells for control and luteolin group, respectively, Fig. 4e and f); 18.07 ± 2.09% for basal vs. 23.13 ± 3.61% for 100 μM luteolin when the cell voltage was held at +40 mV, respectively (p = 0.2554, two-tailed unpaired t-test, n = 9 and 10 cells for control and luteolin group, respectively, Fig. 4e and f). In contrast, we found a 38% and 354%

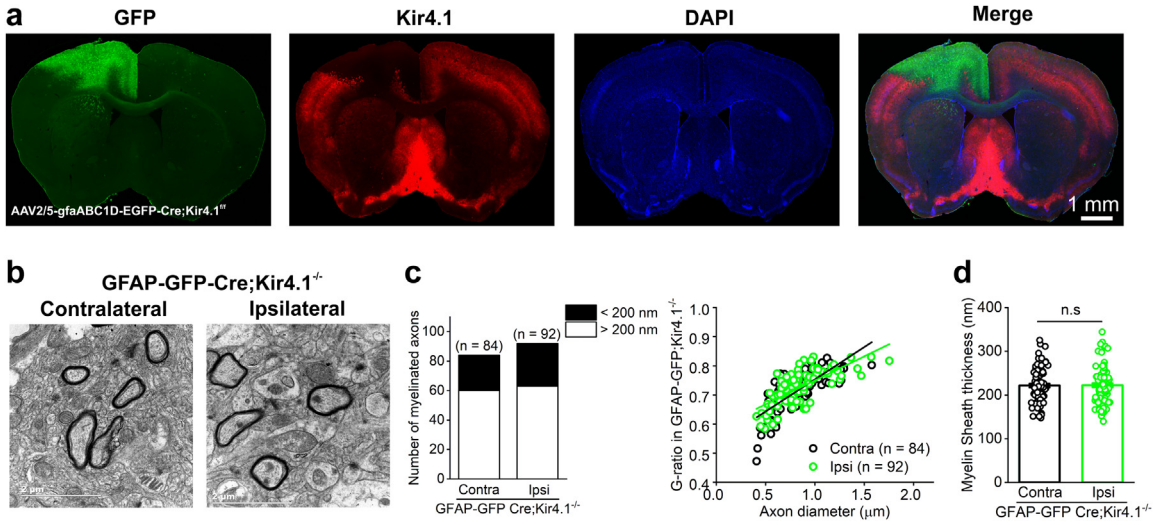

Fig. 3: Deletion of Kir4.1 channels in astrocytes does not lead to myelin loss. (a) Representative images show a complete deletion of Kir4.1 (in red) in GFP (+) astrocytes (in green) of M1 region by injection of Cre-dependent AAV vector (AAV2/5-gfaABC1D-EGFP-P2A-iCre) into Kir4.1$^{f/f}$ mouse cortex. (b) Electron micrographs demonstrate that there is no obvious alteration of myelinated axons between the contralateral (non-injection site) and ipsilateral (astrocytic Kir4.1 deletion site) side in wild type mice at postnatal 8 weeks. Scale bars: 2 μM. (c) Bar graph and G-ratio of myelinated axons represent the number of myelinated axons and G-ratio between ipsilateral M1 cortex with its contralateral side. n indicates the number of axons from 2 GFAP-GFP-Cre;Kir4.1$^{-/-}$ mice. (d) The box-plot represents the average of myelin sheath thickness in contralateral and ipsilateral M1 region in GFAP-GFP-Cre;Kir4.1$^{-/-}$ mice. The data were not normally distributed and statistical significance was assessed using Mann–Whitney unpaired test. n.s indicates not significant. The analyzed axons are from 2 mice.

augmentation of Kir4.1 channel currents in NG2 glia by 100 μM luteolin application when the cell voltage was held at −150 mV and +40 mV respectively, indicating that luteolin has a robust opening effect on Kir4.1 channels specifically expressed in NG2 glia. The net increases of Ba^{2+}-sensitive Kir4.1 currents in NG2 glia were: 81.79 ± 2.33% for basal vs. 112.66 ± 4.90% for 100 μM luteolin when the cell voltage was held at −150 mV ($p < 0.001$, two-tailed unpaired t-test, n = 7 cells for control and luteolin group, respectively, Fig. 4a and b); 13.64 ± 4.89% for basal vs. 61.89 ± 4.59% for 100 μM luteolin when the cell voltage was held at +40 mV, respectively ($p < 0.001$, two-tailed unpaired t-test, n = 7 cells for control and luteolin groups, respectively, Fig. 4a and b). Furthermore, luteolin failed to induce an augmentation of Kir4.1 channel current in Kir4.1 deficient NG2 glia (net increases of Ba^{2+}-sensitive Kir4.1 currents were: 14.21 ± 8.12% for basal vs. 18.41 ± 5.97% for 100 μM luteolin when the cell voltage was held at −150 mV, $p = 0.6784$, two-tailed unpaired t-test, n = 8 and 7 cells for control and luteolin group, respectively; 11.89 ± 2.85% for basal vs. 13.57 ± 2.63% for 100 μM luteolin when the cell voltage was held at +40 mV, respectively, $p = 0.6716$, two-tailed unpaired t-test, n = 8 and 7 cells for control and luteolin groups, respectively, Fig. 4c and d), suggesting that luteolin is a potent Kir4.1 channel activator of NG2 glial cells. Furthermore, we verified the luteolin effects on Kir4.1 protein levels in both purified OPCs and astrocytes following oxygen-glucose deprivation (OGD) *in vitro*. Western blot assay demonstrated that the expression of Kir4.1 was significantly upregulated by luteolin application in OGD-treated OPCs, while the expression of Kir4.1 in OGD-treated astrocytes was unchanged after luteolin application (Fig. S4a–e).

Given this evidence, we next assessed the efficiency of remyelination of axons subjected to luteolin treatment by targeting Kir4.1 channels in tMCAO mice (Figs. 2 and 4a–d). The natural botanical extract luteolin at 35 mg/kg was intraperitoneally injected for 9 consecutive days starting at 24 h reperfusion after the mice underwent tMCAO surgeries (Fig. 6a and Fig. S7).[15,16,28–30] Compared to the ipsilateral region of the saline group in tMCAO mice, luteolin treatment after day 9 increased the number of healthy myelinated axons (myelin sheath > 200 nm) from 15% to 44% (Fig. 5a–d). The remyelination was significantly improved in the luteolin treatment group compared with that in the saline group after 9 days administration in tMCAO mice. The myelin sheath thickness in the saline group was 154.95 ± 4.25 nm in ipsilateral side, vs. 200.22 ± 5.83 nm in ipsilateral side in luteolin group, n = 182 and 165 axons from 5 mice for saline group and 7 mice for luteolin group, respectively, $p < 0.001$, two-tailed unpaired t-test (Fig. 5e). The G-ratio of myelinated axons in saline group after day 9 was

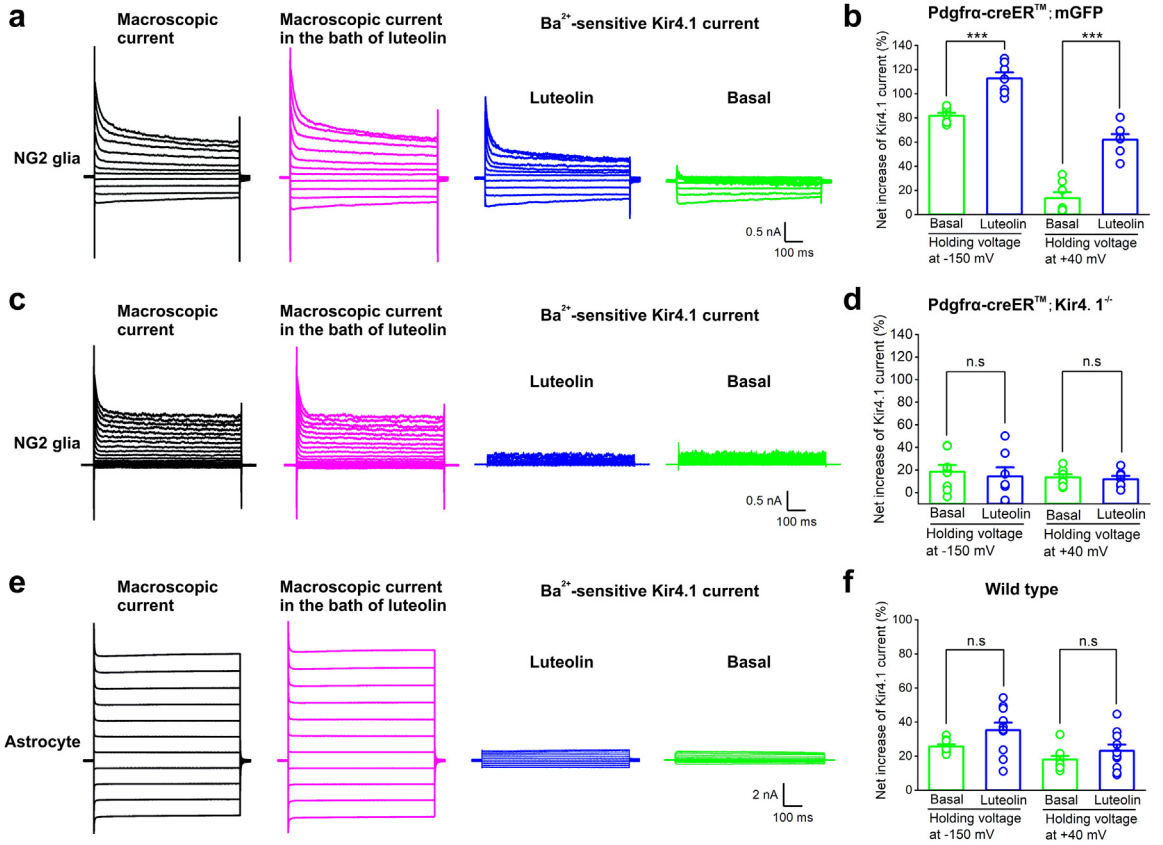

Fig. 4: Luteolin specifically augments Kir4.1 channel currents in NG2 glia. (a) Representative traces show macroscopic current (in black), luteolin-induced macroscopic current (in magenta) and Ba^{2+}-sensitive Kir4.1 currents after luteolin application (in blue) in NG2 glia from Pdgfrα-creER™;mGFP mice. (b) Bar graph summary showing the percentage of augmentation in Ba^{2+}-sensitive Kir4.1 currents between control (basal) and luteolin application when the cell voltage was held at −150 mV and +40 mV, respectively. The error bars represent s.e.m. ***p < 0.001, two-tailed unpaired t-test. n = 7 cells recorded for each group. (c) Representative traces show macroscopic current (in black), luteolin-induced macroscopic current (in magenta) and Ba^{2+}-sensitive Kir4.1 currents after luteolin application (in blue) in NG2 glia from Pdgfrα-creER™; Kir4.1$^{-/-}$ mice. Note that luteolin did not induce the augmentation of Kir4.1 current in NG2 glia in Kir4.1 cKO mice. (d) Bar graph summary showing the percentage of augmentation in Ba^{2+}-sensitive Kir4.1 currents between control (basal) and luteolin application when the cell voltage was held at −150 mV and +40 mV, respectively. The error bars represent s.e.m. n.s indicates not significant, two-tailed unpaired t-test. n = 8 and 7 cells for control and luteolin group, respectively. (e) Representative traces show macroscopic current (in grey), luteolin-induced macroscopic current (in magenta) and Ba^{2+}-sensitive Kir4.1 current after luteolin application (in blue) in astrocytes from wild type mice. (f) Bar graph summary showing the percentage of augmentation in Ba^{2+}-sensitive Kir4.1 currents between control (basal) and luteolin application when the cell voltage was held at −150 mV and +40 mV, respectively. The error bars represent s.e.m. n.s indicates not significant, two-tailed unpaired t-test. n = 9 and 10 cells for control and luteolin group, respectively.

0.8251 ± 0.0048 in ipsilateral side, vs. 0.7644 ± 0.0068 in ipsilateral side in luteolin group, n = 182 and 165 axons from 5 mice for saline group and 7 mice for luteolin group, respectively, p < 0.001, two-tailed unpaired t-test (Fig. 5f). Consistent with the EM results, an enhancement of both Kir4.1 and MBP expression levels was further confirmed in ipsilateral brain region after a 9-days administration of luteolin in tMCAO mice (Fig. 5g and h).

To determine whether luteolin-induced remyelination is mediated by indirectly affecting the Kir4.1 channel through anti-inflammation, anti-apoptosis, or anti-oxidation mechanisms, we did the next series of examinations.[29,31–33] First, we analyzed the amount of microglial activation, which is commonly characterized by CD68 activation in Iba1-labeled microglia. The immunohistochemistry results showed that there was no significant change of microglial activation between the saline group and luteolin group in hippocampus after tMCAO (the percentage of $CD68^{+}$ $Iba1^{+}$ cells in total $Iba1^{+}$ microglia: saline group, 28.07 ± 6.51%, n = 3 mice, luteolin group, 25.93 ± 5.66%, n = 5 mice, p = 0.8175, two-tailed unpaired t-test, Fig. S5a–c). However, we found a decreased level of microglial

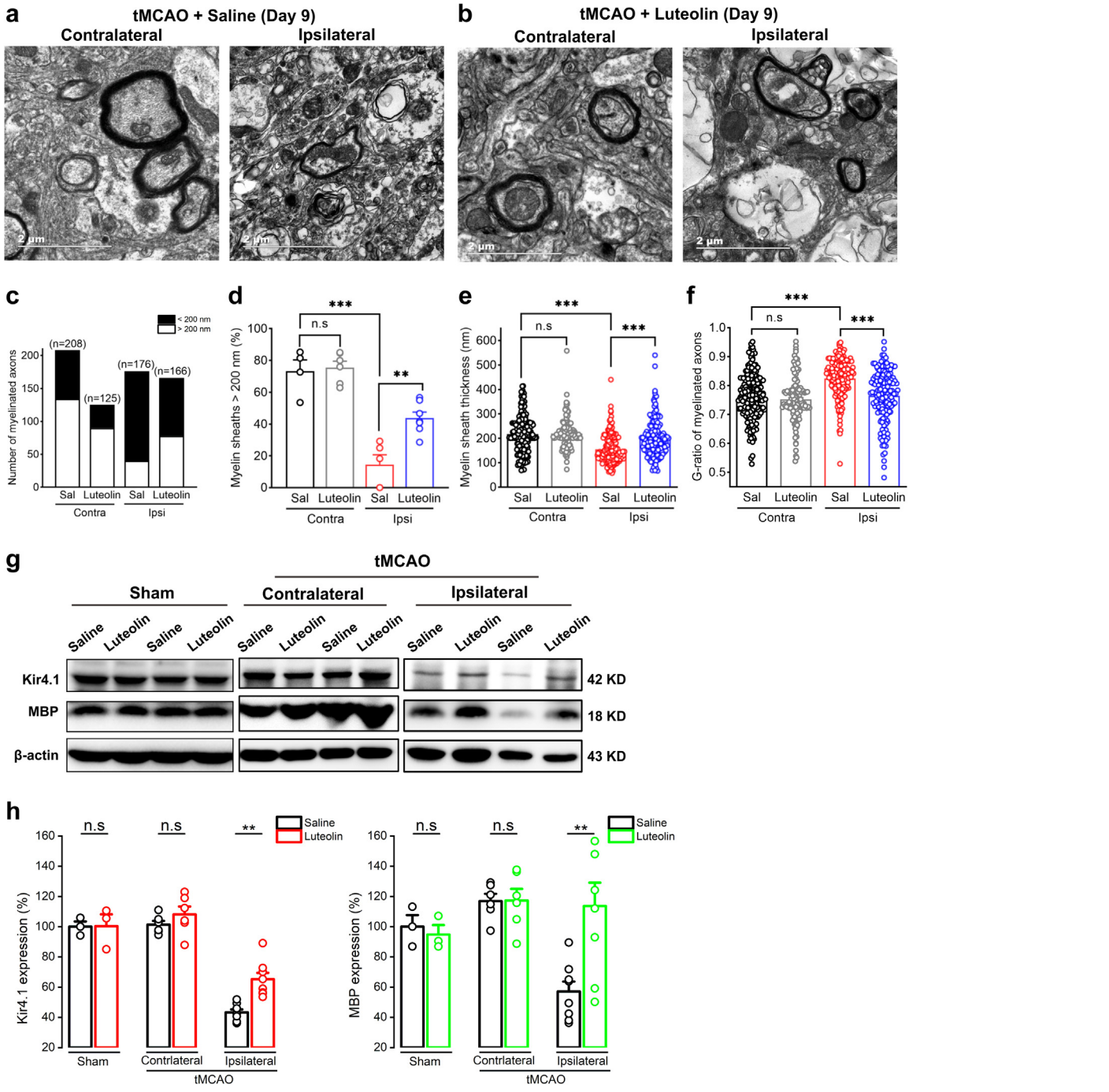

Fig. 5: Luteolin treatment improves remyelination and Kir4.1 expression in tMCAO mice. (a and b) Representative electron micrographs show that the presence of impaired axons with demyelination in ipsilateral cortex compared with its contralateral region at day 9 after tMCAO in wild type mice saline group at postnatal 8 weeks (a) and the remyelinated axons in ipsilateral cortex compared with its contralateral region at day 9 after tMCAO in wild type mice after luteolin treatment at postnatal 8 weeks (b). Scale bars: 2 µM. (c and d) The percentage of healthy axons (the normal diameter of myelinated axons is over 200 nm) between contralateral and ipsilateral cortex after 9 days tMCAO in saline and luteolin group. n indicates the number of axons. The data were normally distributed and statistical significance was assessed within each group using two-tailed unpaired t-test. **p < 0.01; ***p < 0.001, n.s indicates not significant. (e) The box-plots represent average of myelin sheath thickness between saline group and luteolin treatment group after 9 days tMCAO. The data were normally distributed and statistical significance was assessed within each group using two-tailed unpaired t-test. ***p < 0.001, n.s indicates not significant. The analyzed axons are from 6 mice per

activation in the infract core region in M1 cortex after tMCAO (Fig. S5d–f). Secondly, we analyzed the TUNEL-labeled apoptotic cells in both hippocampus and M1 cortex. The immunohistochemistry results showed there was no significant change of TUNEL-labeled cells between the saline group and luteolin group after tMCAO ($p = 0.7029$ for hippocampus, $p = 0.1680$ for M1 cortex, two-tailed unpaired t-test, Fig. S6a–c). Thirdly, we estimated the brain oxidation level with SOD activity assays. The results did not show an obvious increase of SOD levels after luteolin administration in tMCAO mice (Fig. S6d). Taken together, we excluded that the myelin repair by luteolin treatment in ischemia was mediated through an anti-oxidative, anti-apoptotic or anti-inflammatory effect.

Luteolin treatment improves movement capability and neurological functional recovery in ischemic stroke mice

To directly evaluate the outcomes of functional brain recovery in tMCAO mice by luteolin treatment, a series of behavioral tests were sequentially performed at 1, 3, 6 and 9 days after mice received ischemic surgeries. First, we analyzed the infarct volumes after occlusions in tMCAO mice with MRI after luteolin administration at days 1, 3, 6 and 9. Compared with the saline group, the infarct volumes were significantly decreased from 27.63 ± 1.03% to 21.23 ± 0.68% after 6 days luteolin intraperitoneal injection ($p < 0.001$, two-tailed unpaired t-test, $n = 6$ and 7 mice for saline and luteolin groups, respectively, Fig. 6a–c). By day 9, the infarct volumes were further mitigated to 18.55 ± 0.88% in the luteolin group compared to 25.48 ± 1.28% in the saline group ($p < 0.001$, two-tailed unpaired t-test, $n = 6$ and 7 mice for saline and luteolin group, respectively, Fig. 6b and c). Second, we examined the severity of tMCAO mice with corner test performance as indicated in the cartoon (Fig. 6d). As expected, the control mice did not have a preference to turn. However, after being subjected to tMCAO, the animals preferred turning to the left, evidenced by a statistically significant change in laterality index. Further, the ischemic mice treated with luteolin showed a trending improvement of 71.14 ± 2.96% at day 6 and 60.57 ± 2.08% at day 9 in laterality index compared with 89.33 ± 2.51% at day 6 and 80.4 ± 2.71% at day 9 of its saline control ($p < 0.001$ for D6, $p < 0.001$ for D9, two-tailed unpaired t-test, $n = 6$ and 7 mice for saline and luteolin group, respectively, Fig. 6e). Third, we assessed the effect on sensorimotor functions including grid walk and rotarod test. As shown in Fig. 6f and g, the ischemic mice under luteolin treatment after day 6 demonstrated a better placement of their impaired left forelimbs/hindlimbs by significantly decreasing their footfalls when they freely walked on the grid squares compared with those in the saline group (40.01 ± 2.33% of foot falls in saline group vs. 24.75 ± 1.13% foot falls in luteolin group, $p < 0.001$, two-tailed unpaired t-test, $n = 6$ and 7 mice for saline and luteolin group, respectively, Fig. 6f and g and Movies S1–S4). Moreover, the rotarod performance showed luteolin administration after day 6 significantly improved the motor ability of ischemic mice when they were placed on an accelerating rotating rod (Fig. 6h and i). Fourth, the modified neurological severity score (mNSS) was performed to assess the mouse motor, sensory, balance and reflex behaviors.[24,34] In the severity injury scores, 1 score point reflected the inability to perform the test. Therefore, the higher score, the more severe the injury. As shown in Fig. 6j, the tMCAO mice after 6 days administration of luteolin showed a distinct neurological improvement compared with those in the saline group ($p = 0.0023$, 0.0082 for day 6 and day 9, two-tailed unpaired t-test, $n = 6$ and 7 mice for saline and luteolin group, respectively), which indicated the luteolin treatment overall improved the motor abilities and neurological functional recovery in tMCAO mice at the short 6-days period. Fifth, the survival analysis also confirmed an increased longevity of stroke mice from 53% to 73% under a 9-day-period of luteolin treatment (Fig. 6k).

Lastly, we verified the luteolin effects on the functional recovery of ischemic mice occur through the activation of Kir4.1 channels. In conditional Kir4.1 knockout mice (Pdgfrα-creER™;Kir4.1$^{f/f}$), we found that luteolin administration failed to alleviate the infarction volume of Kir4.1 cKO mice after tMCAO on day 3 (Fig. S8a and b). Even worse, the Kir4.1 deficient mice after tMCAO exhibited a very high mortality rate (100%) after day 6, indicating that luteolin lost the binding target for brain repair when kcnj10-encoded Kir4.1 channel was genetically deleted in NG2 glia *in vivo* (Fig. S8c and d).

group. (f) The box-plots represent average G-ratio of myelinated axons between saline group and luteolin treatment group after 9 days tMCAO. The data were normally distributed and statistical significance was assessed within each group using two-tailed unpaired t-test. ***$p < 0.001$, n.s indicates not significant. The analyzed axons are from 6 mice per group. (g) Representative images of Kir4.1 and MBP protein expression in sham and tMCAO mice (contralateral and ipsilateral sides) after 9 days luteolin treatment. Note that both Kir4.1 and MBP expressions are significantly increased in ipsilateral sides after luteolin administration in tMCAO mice compared with its saline group. (h) Summary graphs show the average of Kir4.1 and MBP expressions by Western blot in sham mice and both contralateral and ipsilateral sides of tMCAO mice after 9 days luteolin treatment. **$p < 0.01$, n.s indicates not significant, $n = 3$ mice for both saline and luteolin group in sham control; $n = 6$ mice for both saline and luteolin group in contralateral side after tMCAO; $n = 8$ mice for both saline and luteolin group in ipsilateral side after tMCAO, one-way analysis of variance (ANOVA) followed by Bonferroni *post-hoc* tests.

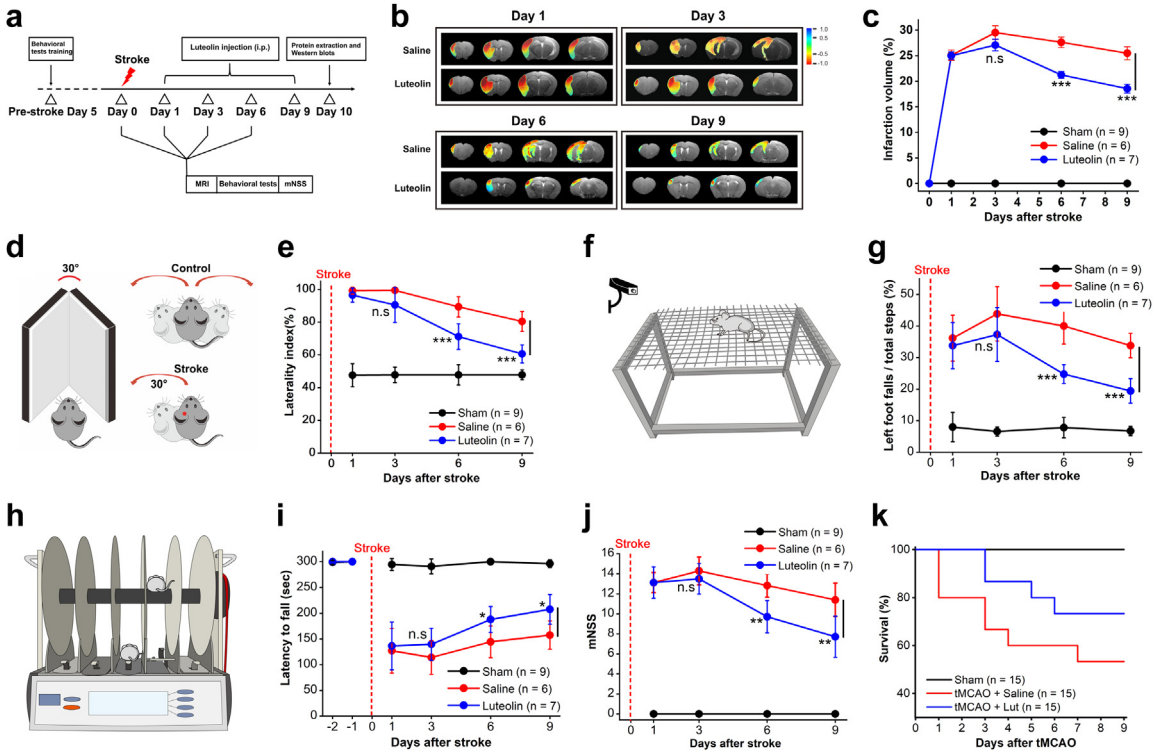

Fig. 6: Luteolin treatment improves motor function and promotes neurological functional recovery in ischemic stroke mice. (a) Experimental diagram showing the procedure for examining the effect of luteolin administration *in vivo* with a series of behavioral tests after the mice underwent ischemic stroke surgeries. (b and c) Representative images of magnetic resonance imaging (MRI) (b) and summary graph (c) of the infarct volumes after occlusions in tMCAO mice after luteolin and its control (saline) administration at days 1, 3, 6 and 9, respectively. Note that after day 6, intraperitoneal injection of luteolin significantly decreases the infarction volumes in tMCAO mice. ***p < 0.001, n.s indicates not significant, two-tailed unpaired t-test. n represents the number of mice examined per group. (d) Schematic cartoon illustrates the severity of tMCAO mouse regarding corner test performance. As expected, the mouse of sham control does not have a preference to turn. After the mouse receives tMCAO, the animal prefers to turn left as evidenced by a significant increase of laterality index. (e) Summary graph shows a trend for improvement of the severity in tMCAO mice with luteolin treatment starting at day 6 compared with the saline group. ***p < 0.001, n.s indicates not significant, two-tailed unpaired t-test. n represents the number of mice examined per group. (f) Schematic cartoon illustrates the motor ability of tMCAO mouse in the grid-walking performance test. (g) Summary graph shows tMCAO mice under luteolin treatment after day 6 demonstrating a better placement of their impaired left forelimbs/hindlimbs by decreasing their footfalls when they freely walked on the grid squares compared with the saline group. ***p < 0.001, two-tailed unpaired t-test, n.s indicates not significant, n = 6 and 7 mice for saline and luteolin group, respectively. (h) Schematic cartoon illustrates sensorimotor function of tMCAO mouse during rotarod test performance. (i) Summary graph shows tMCAO mice under luteolin treatment after day 6 demonstrating a prolonged latency to fall when they were placed on an accelerating rotating rod. *p < 0.05, two-tailed unpaired t-test, n.s indicates not significant, n = 6 and 7 mice for saline and luteolin group, respectively. (j) Summary graph showing the modified neurological severity score (mNSS) to assess the mice motor, sensory, balance and reflex behaviors. 1 score point reflects the inability to perform the test and 16 score point indicates the worst severity of the injury. The tMCAO mice after 6 days administration of luteolin overall show a better neurological improvement compared with the saline group. **p < 0.01, two-tailed unpaired t-test, n.s indicates not significant, n = 6 and 7 mice for saline and luteolin group, respectively. (k) Summary graph of survival curve shows a 73% survival rate of tMCAO mice under a 9-day-period of luteolin treatment compared with a 53% survival rate of tMCAO mice in saline group. n = 15 mice for per group.

Discussion

The present work demonstrates that a dramatic reduction of Kir4.1 channel protein and a severe myelin loss occurs in acute ischemic patients as well as in ischemic stroke model mice. Specific activation of Kir4.1 channels in NG2 glia by luteolin, a natural botanical extract ameliorates the infarction area, promotes remyelination of axons, improves motor function and prolongs the lifespan of ischemic injured mice. Thus, targeting of Kir4.1 ion channels in NG2 glial cells sheds light on a new path for neuronal protection in ischemic injury and luteolin treatment provides a viable venue for the treatment of ischemic stroke.

A plethora of neurological disorders share a final common lethally pathway known as excitotoxicity. Among these disorders, ischemic stroke is a prevalent

cause of death and disability worldwide. Brain ischemia stems from cardiac arrest or stroke, which are responsible for insufficient blood supply to the brain parenchyma. Glucose and oxygen deficiency disrupts oxidative phosphorylation and results in energy depletion and ionic imbalance, followed by cell membrane depolarization, calcium overload and/or extracellular accumulation of the excitatory amino acid glutamate. Glial cells, including astrocytes and NG2 glia (also known as OPCs), constitute 90% of neural cell populations in the mammalian brain. Numerous studies have shown that the function of glial cells is not only for supporting adjacent neurons with nutrients and metabolic shuttling, but also for maintaining the homeostasis of K^+ in the extracellular space, scavenging of accumulated neurotransmitters and actively interacting with neuronal synapses.[6,11,35] Thus, glial cells can act as protectors of the CNS, as well as initiators and propagators of ischemic injury.[36] In fact, oligodendrocyte lineage cells are more vulnerable to oxidative stress and hypoxia than any other type of glial cells.[4,5,37] Our study first provided evidence that Kir4.1 channels and myelin sheath of axons are largely impaired in ischemic cerebral cortex of human patients (Fig. 1a–c). Consistent with the results from human brain tissue, we further confirmed that the deficits of Kir4.1 ion channels expressed in NG2 glia but not in astrocytes contributed to an initial response in tMCAO mice (Fig. 2a–c, Fig. S1 and S2).

Kir4.1 channel represents one of the most prominently expressed ion channels in adult NG2 glia, which determines the resting membrane potential of these cells, as well as a regulator during the maturation of oligodendrocytes.[4,5,38,39] Studies obtained from oligodendrocytes in the white matter suggest that Kir4.1 is critical to extracellular K^+ homeostasis and axonal electrical conduction.[13] In pathological conditions, Kir4.1 could serve as a potential therapeutic candidate in mediating secondary effects of CNS injury. By inhibiting Kir4.1 channels, OPC differentiation and oligodendrocyte maturation are both impeded, which might be due to Kir4.1 altering the intracellular pH of oligodendrocyte lineage cells through Na^+/H^+ exchangers during development.[40] In our study, we found that the deficits of Kir4.1 channel in ischemia could cause adult NG2 glia depolarization and dampen the ability of K^+ siphoning, which subsequently induce neuron deterioration through excitotoxicity due to an enhanced extracellular K^+ level and/or glutamate accumulation.[10,11] More importantly, the impairment of Kir4.1 channels in NG2 glia instead of oligodendrocytes can directly induce myelin loss of axons, which is ultimately unable of supporting neuronal saltatory conduction of electric impulses and causes a dual effect on the aggravation of the neuronal loss and/or death.[41] Up to date, there is no evidence showing that kcnj10 encodes a protein of myelin synthesis/degradation, nor with a protein involved in the immune response to myelin.[8] Thus, it would be interesting to illuminate the detailed mechanism of how Kir4.1 channel impacts a myelin protein such as MBP in future studies. Overall, Kir4.1 channels possibly play a crucial role in the pathogenesis of ischemic stroke and could be a key factor to be targeted to cure such a disease.

Increasing evidence has shown that luteolin is one of the natural polyphenols with anti-oxidative, anti-mutagenic, anti-apoptotic and anti-inflammatory properties.[29,31–33,42] Therefore, luteolin has been reported to prevent neuronal damage from ischemic injuries through various signaling pathways as follows: 1) luteolin activates antioxidant compounds to promote the reduction of neuronal cell death in an ischemic rat model[43]; 2) luteolin binds to PPARγ and reduces the infarct area in MCAO-treated rats through inhibition of secretion of inflammatory cytokines[44,45]; 3) luteolin regulates an anti-apoptosis key protein AKT or increases the expression of BCL-2 to suppress the apoptotic process in ischemia-reperfusion injury.[44,46] Although the aforementioned progress on luteolin as ischemic remedy, a systematic study on ischemia from humans to rodents has not been fully elucidated. Interestingly, in coronary arterial spasm, luteolin has recently been found to prevent the various vasoconstrictors by augmenting both Kv and Kir channel currents in rat coronary arterial smooth muscle cells (RCASMCs).[20] 300 μM Ba^{2+} reduced 100 μM luteolin-induced net Kir current increase by 42% at a holding rest membrane potential of –140 mV.[20] In adult mouse hippocampal acute slices, our study showed a similar augmentation of Kir4.1 channel currents by 38% with 100 μM luteolin application in NG2 glia at a holding voltage of –150 mV, indicating luteolin exhibits a new function as K^+ channel activator in the brain. Surprisingly, when comparing the Kir4.1 currents at a holding voltage of +40 mV by increasing K^+ ion driving force to the glial cells at a hyperpolarized resting membrane potential,[10] NG2 glia showed a dramatic increased in Kir4.1 currents to 3.5 fold after luteolin application compared to a 0.28 fold increase in astroglia, which is most likely due to an undefined specific activation site of Kir4.1 channel expressed in NG2 glia. Although there is an absolute higher amount of Kir4.1 mRNA expression in astroglia than that in oligodendrocyte lineage cells including NG2 glia, the Ba^{2+}-sensitive Kir4.1 channel currents contribute to 82% and 26% of total macroscopic K^+ currents in NG2 glia and astrocytes respectively in adult acute hippocampal tissues (unpublished data),[5,47] which strongly supports the idea that Kir4.1 channels are heterogeneous in different types of glial cells.[25] Further elucidation of the structural basis of Kir4.1 channels in NG2 glia would be more informative and merits further

investigation for identifying the specific channel opening site and its efficiency activated by luteolin.

In diabetic cataracts, luteolin derivatives have been revealed as a new potential druggable target for the inhibition of aldose reductase based on a structure–activity relationship study.[48] The pharmacokinetic evaluation of the clinical interactions and our animal study indicated that luteolin derivatives are more likely to be membrane permeable and easily absorbed by the body and are suitable to be used as drugs as per Lipinski's rule of four criteria such as human intestinal absorption (HIA), skin permeability (SP), blood brain barrier (BBB) penetration and plasma protein binding (PPB) (Fig. S7).[48] Flavonols such as luteolin, quercetin, kaempferol, and myricetin are the most abundant flavonoids in plant foods and are mainly present in leafy vegetables, apples, onions, broccoli, and berries. Although dietary flavonoid intake for cancer prevention remains controversial,[49,50] the median intake of luteolin at the dose of 0.20 mg/day didn't show any side effects from the intake of flavonoid-rich foods in a cardiovascular disease and cancer disease cohort study.[51] Instead, in an exercise performance case study, twelve healthy male physical students showed an enhancement of performance, muscle O_2 extraction, and brain oxygenation during sprint exercise and post-exercise ischemia after they received 100 mg/day of peanut husk extract containing 95% luteolin in both acute and prolonged effects.[29] Therefore, supplementation with a botanical extract of luteolin has been proved as a promising food additive and has biosafety in humans. Most importantly, as evidence from electrophysiological, cellular and behavioral levels we provided aforementioned in this study, luteolin and its potential derivatives can be a powerful druggable candidate for the treatment of ischemic stroke patients to prevent demyelination of axons and facilitate prompt functional brain recovery after acute ischemic injury.

Contributors

X.H., Y.J., S.D., X.Z., H.Z., B.Z., and C.Z. were responsible for conducting electrophysiology, immunohistochemistry, Western blotting, immunoelectron microscopy and data analysis. X.H. and H.Z. were responsible for HEK-293T cells cultures and Kir4.1 plasmid transfection. Y.J., B.Z., S.D. and J.Z. carried out behavioral experiments, animal breeding and human tissue collection. X.T. and J.W. directed the work and X.T. wrote the paper. X.T. and J.W. have accessed and verified the underlying data. All authors have read and approved the final version of the manuscript.

Data sharing statement

All the data during the current study have been shown in the manuscript and supplemental materials, and unprocessed data are available from the corresponding author on reasonable request.

Declaration of interests

The authors declare no competing interests.

Acknowledgments

This work was supported by grants from the Ministry of Science and Technology China Brain Initiative (2022ZD0204702, to X.T.), the National Natural Science Foundation of China (82271466, 82171279, 31970904 and 31571063), the Program for Professor of Special Appointment (Eastern Scholar for Dr. X.T.) at Shanghai Institutions for Higher Learning (1510000084), Shanghai Municipal Science and Technology Major Project (2018SHZDZX05) and Shanghai Science and Technology Project (17411954000). We thank Ms. Chenyu Yang for the technical assistance on electron microscopy (Center of Cryo-electron Microscopy, Zhejiang University, China). We thank Prof. Carlos Cepeda (David Geffen School of Medicine, University of California Los Angeles, CA, USA) for fruitful discussions and critical comments of our paper. We thank the innovative research team of high-level local universities in Shanghai for their support (SHSMU-ZDCX20211901, SHSMU-ZDCX20211100).

Appendix A. Supplementary data

Supplementary data related to this article can be found at https://doi.org/10.1016/j.ebiom.2022.104406.

References

1 Hacke W, Kaste M, Fieschi C, et al. Intravenous thrombolysis with recombinant tissue plasminogen activator for acute hemispheric stroke: the European Cooperative Acute Study (ECASS). *JAMA*. 1995;274(13):1017–1025.
2 Sandercock P, Wardlaw JM, Lindley RI, et al. The benefits and harms of intravenous thrombolysis with recombinant tissue plasminogen activator within 6 h of acute ischaemic stroke (the third international stroke trial IST-3): a randomised controlled trial. *Lancet*. 2012;379(9834):2352–2363.
3 National Institute of Neurological Disorders and Stroke rt-PA Stroke Study Group. Tissue plasminogen activator for acute ischemic stroke. *N Engl J Med*. 1995;333(24):1581–1587.
4 Song FE, Huang JL, Lin SH, Wang S, Ma GF, Tong XP. Roles of NG2-glia in ischemic stroke. *CNS Neurosci Ther*. 2017;23(7):547–553.
5 Song F, Hong X, Cao J, et al. Kir4.1 channels in NG2-glia play a role in development, potassium signaling, and ischemia-related myelin loss. *Commun Biol*. 2018;1:80.
6 Zhang X, Liu Y, Hong X, et al. NG2 glia-derived GABA release tunes inhibitory synapses and contributes to stress-induced anxiety. *Nat Commun*. 2021;12(1):5740.
7 Kofuji P, Ceelen P, Zahs KR, Surbeck LW, Lester HA, Newman EA. Genetic inactivation of an inwardly rectifying potassium channel (Kir4.1 subunit) in mice: phenotypic impact in retina. *J Neurosci*. 2000;20(15):5733–5740.
8 Neusch C, Rozengurt N, Jacobs RE, Lester HA, Kofuji P. Kir4.1 potassium channel subunit is crucial for oligodendrocyte development and in vivo myelination. *J Neurosci*. 2001;21(15):5429–5438.
9 Djukic B, Casper KB, Philpot BD, Chin LS, McCarthy KD. Conditional knock-out of K(ir)4.1 leads to glial membrane depolarization, inhibition of potassium and glutamate uptake, and enhanced short-term synaptic Potentiation. *J Neurosci*. 2007;27(42):11354–11365.
10 Maldonado PP, Velez-Fort M, Levavasseur F, Angulo MC. Oligodendrocyte precursor cells are accurate sensors of local K^+ in mature gray matter. *J Neurosci*. 2013;33(6):2432–2442.
11 Tong XP, Ao Y, Faas GC, et al. Astrocyte Kir4.1 ion channel deficits contribute to neuronal dysfunction in Huntington's disease model mice. *Nat Neurosci*. 2014;17(5):694–703.
12 Nwaobi SE, Cuddapah VA, Patterson KC, Randolph AC, Olsen ML. The role of glial-specific Kir4.1 in normal and pathological states of the CNS. *Acta Neuropathol*. 2016;132(1):1–21.
13 Schirmer L, Mobius W, Zhao C, et al. Oligodendrocyte-encoded Kir4.1 function is required for axonal integrity. *Elife*. 2018;7:21.
14 Carlson AP, McKay W, Edwards JS, et al. MicroRNA analysis of human stroke brain tissue resected during decompressive craniectomy/stroke-ectomy surgery. *Genes (Basel)*. 2021;12(12):1860.
15 Ziyan L, Yongmei Z, Nan Z, Ning T, Baolin L. Evaluation of the anti-inflammatory activity of luteolin in experimental animal models. *Planta Med*. 2007;73(3):221–226.

16 Xu J, Wang H, Ding K, et al. Luteolin provides neuroprotection in models of traumatic brain injury via the Nrf2-ARE pathway. *Free Radic Biol Med*. 2014;71:186–195.
17 Yang W, He S, Xiao N, et al. Simultaneous determination of 15 flavonoids in scutellaria barbata-hedyotis diffusa herb pair by HPLC Q-TOF MS. *J AOAC Int*. 2019;102:75–80.
18 Watanabe H, Sano H, Chiken S, et al. Forelimb movements evoked by optogenetic stimulation of the macaque motor cortex. *Nat Commun*. 2020;11(1):3253.
19 Battefeld A, Klooster J, Kole MHP. Myelinating satellite oligodendrocytes are integrated in a glial syncytium constraining neuronal high-frequency activity. *Nat Commun*. 2016;7:13.
20 Li WP, Dong MM, Guo PM, et al. Luteolin-induced coronary arterial relaxation involves activation of the myocyte voltage-gated K^+ channels and inward rectifier K^+ channels. *Life Sci*. 2019;221:233–240.
21 Baskin YK, Dietrich WD, Green EJ. Two effective behavioral tasks for evaluating sensorimotor dysfunction following traumatic brain injury in mice. *J Neurosci Methods*. 2003;129(1):87–93.
22 Zhang L, Schallert T, Zhang ZG, et al. A test for detecting long-term sensorimotor dysfunction in the mouse after focal cerebral ischemia. *J Neurosci Methods*. 2002;117(2):207–214.
23 Shiotsuki H, Yoshimi K, Shimo Y, et al. A rotarod test for evaluation of motor skill learning. *J Neurosci Methods*. 2010;189(2):180–185.
24 Li Y, Chopp M, Chen JL, et al. Intrastriatal transplantation of bone marrow nonhematopoietic cells improves functional recovery after stroke in adult mice. *J Cereb Blood Flow Metab*. 2000;20(9):1311–1319.
25 Tang XF, Taniguchi K, Kofuji P. Heterogeneity of Kir4.1 channel expression in glia revealed by mouse transgenesis. *Glia*. 2009;57(16):1706–1715.
26 Miean KH, Mohamed S. Flavonoid (myricetin, quercetin, kaempferol, luteolin, and apigenin) content of edible tropical plants. *J Agric Food Chem*. 2001;49(6):3106–3112.
27 Ross JA, Kasum CM. Dietary flavonoids: bioavailability, metabolic effects, and safety. *Annu Rev Nutr*. 2002;22:19–34.
28 Park S, Lim W, You S, Song G. Ameliorative effects of luteolin against endometriosis progression in vitro and in vivo. *J Nutr Biochem*. 2019;67:161–172.
29 Gelabert-Rebato M, Wiebe JC, Martin-Rincon M, et al. Enhancement of exercise performance by 48 hours, and 15-day supplementation with mangiferin and luteolin in men. *Nutrients*. 2019;11(2):23.
30 Park CM, Song YS. Luteolin and luteolin-7-O-glucoside protect against acute liver injury through regulation of inflammatory mediators and antioxidative enzymes in GalN/LPS-induced hepatitic ICR mice. *Nutr Res Pract*. 2019;13(6):473–479.
31 Lu XY, Li YH, Li XB, Aisa HA. Luteolin induces apoptosis in vitro through suppressing the MAPK and PI3K signaling pathways in gastric cancer. *Oncol Lett*. 2017;14(2):1993–2000.
32 Jia ZQ, Nallasamy P, Liu DM, et al. Luteolin protects against vascular inflammation in mice and TNF-alpha-induced monocyte adhesion to endothelial cells via suppressing IKB alpha/NF-kappa B signaling pathway. *J Nutr Biochem*. 2015;26(3):293–302.
33 Luo YY, Shang PP, Li DY. Luteolin: a flavonoid that has multiple cardio-protective effects and its molecular mechanisms. *Front Pharmacol*. 2017;8:10.
34 Chen JL, Li Y, Wang L, et al. Therapeutic benefit of intravenous administration of bone marrow stromal cells after cerebral ischemia in rats. *Stroke*. 2001;32(4):1005–1011.
35 Takano T, Oberheim N, Cotrina ML, Nedergaard M. Astrocytes and ischemic injury. *Stroke*. 2009;40(3):S8–S12.
36 Kirdajova DB, Kriska J, Tureckova J, Anderova M. Ischemia-triggered glutamate excitotoxicity from the perspective of glial cells. *Front Cell Neurosci*. 2020;14:27.
37 Husain J, Juurlink BHJ. Oligodendroglial precursor cell susceptibility to hypoxia is related to poor ability to cope with reactive oxygen species. *Brain Res*. 1995;698(1–2):86–94.
38 Higashimori H, Sontheimer H. Role of Kir4.1 channels in growth control of glia. *Glia*. 2007;55(16):1668–1679.
39 Larson VA, Zhang Y, Bergles DE. Electrophysiological properties of NG2(+) cells: matching physiological studies with gene expression profiles. *Brain Res*. 2016;1638(Pt B):138–160.
40 Wang N, Zhou L, Shao CY, et al. Potassium channel Kir 4.1 regulates oligodendrocyte differentiation via intracellular pH regulation. *Glia*. 2022;70(11):2093–2107.
41 Larson VA, Mironova Y, Vanderpool KG, et al. Oligodendrocytes control potassium accumulation in white matter and seizure susceptibility. *Elife*. 2018;7:33.
42 Cook MT, Liang YY, Besch-Williford C, Hyder SM. Luteolin inhibits lung metastasis, cell migration, and viability of triple-negative breast cancer cells. *Breast Cancer*. 2017;9:9–19.
43 Zhang YC, Gan FF, Shelar SB, Ng KY, Chew EH. Antioxidant and Nrf2 inducing activities of luteolin, a flavonoid constituent in Ixeris sonchifolia Hance, provide neuroprotective effects against ischemia-induced cellular injury. *Food Chem Toxicol*. 2013;59:272–280.
44 Qiao H, Dong L, Zhang X, et al. Protective effect of luteolin in experimental ischemic stroke: upregulated SOD1, CAT, Bcl-2 and claudin-5, down-regulated MDA and Bax expression. *Neurochem Res*. 2012;37(9):2014–2024.
45 Li L, Pan G, Fan R, et al. Luteolin alleviates inflammation and autophagy of hippocampus induced by cerebral ischemia/reperfusion by activating PPAR gamma in rats. *BMC Complement Med Ther*. 2022;22(1):176.
46 Tan L, Liang C, Wang Y, Jiang Y, Zeng S, Tan R. Pharmacodynamic effect of luteolin micelles on alleviating cerebral ischemia reperfusion injury. *Pharmaceutics*. 2018;10(4):248.
47 Zhang Y, Chen KN, Sloan SA, et al. An RNA-sequencing transcriptome and splicing database of glia, neurons, and vascular cells of the cerebral cortex. *J Neurosci*. 2014;34(36):11929–11947.
48 Sebastian J. Structure-activity relationship study reveals benzazepine derivatives of luteolin as new aldose reductase inhibitors for diabetic cataract. *Curr Drug Discov Technol*. 2016;13(3):152–163.
49 Le Marchand L, Murphy SP, Hankin JH, Wilkens LR, Kolonel LN. Intake of flavonoids and lung cancer. *J Natl Cancer Inst*. 2000;92(2):154–160.
50 Christensen KY, Naidu A, Parent ME, et al. The risk of lung cancer related to dietary intake of flavonoids. *Nutr Cancer*. 2012;64(7):964–974.
51 Wang L, Lee IM, Zhang SM, Blumberg JB, Buring JE, Sesso HD. Dietary intake of selected flavonols, flavones, and flavonoid-rich foods and risk of cancer in middle-aged and older women. *Am J Clin Nutr*. 2009;89(3):905–912.